Impact of Eurasian autumn snow on the winter North Atlantic Oscillation in seasonal forecasts of the 20th century.

Martin Wegmann[1,2,3], Yvan Orsolini[4], Antje Weisheimer[5,6], Bart van den Hurk[6,7] and Gerrit Lohmann[3]

[1]Institute of Geography, University of Bern, Bern, Switzerland.
[2]Oeschger Centre for Climate Change Research, University of Bern, Bern, Switzerland.
[3]Alfred-Wegener-Institute, Helmholtz Center for Polar and Marine Research, Bremerhaven, Germany
[4]NILU–Norwegian Institute for Air Research, Kjeller, Norway
[5]National Centre for Atmospheric Science, Atmospheric, Oceanic and Planetary Physics, University of Oxford, Oxford, United Kingdom
[6]European Centre for Medium-Range Weather Forecasts, Reading, United Kingdom
[7]Deltares, Delft, The Netherlands

Corresponding author: Martin Wegmann, Institute of Geography and Oeschger Centre for Climate Change Research, University of Bern, Hallerstrasse 12, 3012 Bern, Switzerland. Email: martin.wegmann@giub.unibe.ch

Key points

Snow–atmosphere coupling, seasonal prediction, North Atlantic Oscillation, polar vortex, stratospheric warming, hindcast

Abstract

As the leading climate mode of wintertime climate variability over Europe, the North Atlantic Oscillation (NAO) has been extensively studied over the last decades. Recently, studies highlighted the state of the Eurasian cryosphere as a possible predictor for the wintertime NAO. However, missing correlation between snow cover and wintertime NAO in climate model experiments and strong non-stationarity of this link in reanalysis data is questioning the causality of this relationship.

Here we use the large ensemble of Atmospheric Seasonal Forecasts of the 20th Century (ASF-20C) with the European Centre for Medium-Range Weather Forecasts model, focusing on the winter season. Besides the main 110-year ensemble of 51 members, we investigate a second, perturbed ensemble of 21 members where initial (November) land conditions over the Northern Hemisphere are swapped from neighboring years. The Eurasian snow / NAO linkage is examined in terms of a longitudinal snow depth dipole across Eurasia. Subsampling the perturbed forecast ensemble and contrasting members with high and low initial snow dipole conditions, we found that their composite difference indicates more negative NAO states in the following winter (DJF) after positive west to east snow depth gradients at the beginning of November. Surface and atmospheric forecast anomalies through the troposphere and stratosphere associated with the anomalous positive snow dipole consist of colder early winter surface temperatures over Eastern Eurasia, an enhanced Ural ridge and increased vertical energy fluxes into the stratosphere, with a subsequent negative NAO-like signature in the troposphere. We thus confirm the existence of a causal connection between autumn snow patterns and subsequent winter circulation in the ASF-20C forecasting system.

1. Introduction

As the leading climate variability pattern affecting winter climate over Europe, the North Atlantic Oscillation (NAO) has been extensively studied over the last decades (Wanner et al., 2001; Hurrell and Deser, 2010; Moore and Renfrew, 2012; Deser et al., 2017). The NAO state strongly impacts the hydroclimate as well as the ecological and socioeconomic conditions over major population clusters of Europe and North America. In its positive state, the NAO projects onto strong pressure gradients over the North Atlantic, strong westerly winds and mild but wet conditions for Central Europe. A negative winter NAO is connected to a southwardly displaced Atlantic jet stream, weaker westerlies and cold, dry conditions for Central Europe. The NAO also shows a distinct quadrupole signature in surface temperature straddling the Atlantic, with two opposite poles over northern Europe and Greenland /Labrador and an opposite pair further south over southern Europe/North Africa and the US East Coast. Recent cases of extreme negative NAO states (Wang and Chen, 2010; Lü et al., 2020), including the winter 2020/2021, coincided with several extreme weather events across the Northern Hemisphere, including cold air outbreaks with record snowfall at locations over Southern and Northern Europe, as well as eastern parts of Canada and the United States (Blunden and Boyer, 2021).

Improving seasonal to decadal predictions of the winter NAO is a high priority research for many weather and climate related research centres (Kang et al., 2014; Scaife et al., 2014, 2016; Smith et al., 2016; Dunstone et al., 2016; Athanasiadis et al., 2017; Weisheimer et al., 2017; Baker et al., 2018; Weisheimer et al., 2019). Despite its stochastic behaviour, the NAO state was shown to be modulated by slowly varying components of the climate system, carrying the climate state "memory" across months or even seasons (Dobrynin et al., 2018; Meehl et al., 2021). Initially discussed by Cohen and Enthekhabi (1999), recent studies have highlighted the potential of Eurasian autumn snow cover anomalies as a useful predictor for the boreal wintertime (December– January–February, DJF) NAO in empirical prediction models (Cohen et al., 2007, 2014; Cohen and Jones 2011; Peings et al., 2013; Tian and Fan 2015; Wang et al., 2017; Han and Sun 2018; Wegmann et al., 2020).

The causal chain behind the snow impact is hypothesized as follows: due to the radiative and thermodynamical properties of snow (Cohen and Rind 1991; Vavrus 2007; Dutra et al., 2011; Thackeray et al., 2019), a thicker snowpack is associated with coherent surface cooling. Cohen et al. (2007; see also Cohen et al., 2014; Henderson et al., 2018 for reviews) proposed a multi-step mechanism whereby this surface cooling leads to raised isentropic surfaces, triggering increased Rossby wave activity propagating upward and being absorbed in the stratosphere, warming it and subsequently weakening the polar vortex. The negative stratospheric Northern Annular Mode signal eventually propagates down into the troposphere and to the surface where it projects onto a negative NAO.

Investigating the robustness of this mechanism is challenged by several elements. Observational studies analyzing statistical links are restricted by the relatively short length (a few decades) of comprehensive and complete snow cover observations. Using long-term reanalyses, recent studies showed substantial

non-stationary relationships between autumn Eurasian snow cover and the sign of the winter NAO over the span of the 20th century (Peings et al., 2013; Douville et al., 2016; Wegmann et al., 2020). Using shorter time scales, the probability of "cherry picking" a period of positive correlation and sampling co-variability with other climate system components increases considerably. Causes for the non-stationarity are still discussed, with possible influences from the Quasi-Biennial Oscillation (QBO), El Niño-Southern Oscillation (ENSO) or simply snow cover variance (Peings et al., 2017; O'Reilly et al., 2017; Tyrrell et al., 2018; Wegmann et al., 2020; Weisheimer et al., 2020). Disentangling co-variability is further challenged by the co-occurrence of increased Eurasian snow cover and increased Ural blocking frequency, questioning the lead-lag relationship between snow cover and blocking (Peings 2019; Song and Wu, 2019; Santolaria-Otín et al., 2021). Moreover, a variety of temporal and spatial snow cover indices used among the different studies obstructs direct comparisons. Nevertheless, recent studies point out that a November longitudinal snow cover dipole across Eurasia shows the strongest statistical link to the DJF NAO state (Gastineau et al., 2017; Han and Sun 2018; Santolaria-Otín et al., 2021).

Analyzing the snow → NAO mechanism in modelling experiments is challenged by short-comings of the current Atmospheric or Atmosphere-Ocean General Circulation Models (AGCMs or AOGCMs) regarding snow-atmosphere feedbacks (Santolaria-Otín and Zolina 2020). Most of the free-running Coupled-Model Intercomparison Project (CMIP) models do not capture the statistical snow-NAO link found in reanalyses data (Hardimann et al., 2008; Furtado et al., 2015; Gastineau et al., 2017). On the other hand, when large snowpack anomalies are prescribed through nudging or imposed as initial conditions, several AGCM experiments showed promising results for identifying several to all steps of the proposed mechanism (Gong et al., 2003; Fletcher et al., 2009; Peings et al., 2012; Tyrrell et al., 2018).

Some of the current-generation subseasonal-to-seasonal or seasonal coupled prediction models also seem to catch parts of the mechanism chain, specifically negative temperature anomalies associated with a thicker snowpack (Orsolini et al., 2013; Diro and Lin, 2020) as well as an enhanced wave activity generating upward fluxes into the stratosphere associated with ridging over Eurasia (Orsolini et al., 2016; Li et al., 2019; Garfinkel et al., 2020), although several models failed to simulate that ridging in Garfinkel et al. (2020). The subsequent stratosphere-troposphere coupling influencing the surface Arctic Oscillation also tended to be weak to non-existent in most models. These studies have been limited to the recent decades and, consequently, confidence in the robustness of the mechanism across spans of decades is still low and needs to be strengthened (Garfinkel et al., 2020).

To disentangle the issues of non-stationarity (found in observations) and causality (found in models), we base our investigation on a 110-year long (1901-2010) ensemble seasonal prediction experiment, which consists of the historical seasonal hindcasts using ECMWF's atmosphere-only model, called "ASF-20C" (Weisheimer et al., 2017). This 51-member ensemble of hindcasts with four start dates per

year and a length of 4 months has been used in several studies on the predictability of the NAO and other climate patterns (e.g., O'Reilly et al., 2017; Parker et al., 2019; Weisheimer et al., 2019; Weisheimer et al., 2020; O'Reilly et al., 2020). To investigate the influence of land surface conditions, in this case snow cover, on the evolution of the atmospheric state throughout the season, we use a novel, 21-member twin set of the ASF-20C forecasts with perturbed initial land conditions. This dataset was used as a pilot experiment in the context of the Land Surface, Snow and Soil moisture Model Intercomparison Program LS3MIP (Van den Hurk et al., 2016), aimed at reproducing land surface potential predictability experiments as described by Dirmeyer et al. (2013). We aim to address the question of causality, pathway, stationarity and seasonal evolution of the proposed mechanism of the snow-stratosphere-troposphere linkage over decadal to centennial time scales.

This paper is organized as follows. Sect. 2 describes the data and methods used. In Sect. 3, we show winter evolution of climate anomalies for the different initialization runs and contrast them with observed anomalies. The results are discussed in Sect. 4 and finally summarized in Sect. 5.

2. Data and Methods

a. Climate reanalysis and reconstruction

We use the European Centre for Medium-Range Weather Forecasts (ECMWF) product ERA-20C (ERA20C; Poli et al., 2016) to investigate pre-conditions and the initialization of the seasonal predictions, to compute the DJF NAO index as well as to create a Eurasian snow dipole index. ERA-20C only assimilates surface pressure and marine wind observations, with sea surface temperature (SSTs) boundary conditions taken from the HadISST2.1.0.0 datasets (Rayner et al., 2003). ERA-20C was found to represent interannual snow variations over Eurasia remarkably well. For an in-depth discussion of its performance and the technical details concerning snow computation, see Wegmann et al., (2017b). Due to the a-forementioned statistical impact for the winter NAO evolution, we focus on the November Eurasian snow dipole index as a predictor for the following NAO state (Gastineau et al., 2017; Han and Sun 2018; Santolaria-Otín et al., 2021). Following Han and Sun (2018) who explicitly selected western and eastern domains because of the high co-variance with DJF NAO, we calculate the index over the period 1901–2010 by averaging snow depths over the western domain (30°-60°E, 48°N-58°N) and the eastern domain (80°-130°E, 40°-56°N), eventually subtracting the western domain from the eastern domain to derive the west-east snow depth gradient. Hence, a positive snow index indicates higher snow depths in the eastern domain and a positive longitudinal snow depth gradient. The index is normalized and linearly detrended with respect to the overall period. To comply with the initialization date of 1st of November for the seasonal hindcasts, we calculate the index for 1st of November instead of November mean snow (Figure 1a). Even though Han and Sun (2018) calculated the dipole index using snow cover, we used snow depth since ERA-20C provides snow depth as the actual prognostic variable. We hence refrained from using empirical rules to convert snow depth to snow cover. We found the index based on snow depth to be virtually identical (also see Supplementary Figure S1) to the index using snow cover (see also Wegmann et al., 2020 for more insights).

To compute the winter NAO index, we normalize the first Empirical Orthogonal Function of ERA-20C DJF sea level pressure (SLP) for the region (90°-50°E, 20°-80°N). We use the same approach to calculate the NAO DJF index based on the seasonal hindcasts and compare those with the reconstructed, independent DJF NAO index by Jones et al., (1997) from the Climate Research Unit (CRU).

b. Seasonal prediction experiments

Additionally, we use atmospheric seasonal retrospective hindcasts covering the 110-year period 1901-2010 of ERA-20C with 51 ensemble members of the ASF-20C hindcasts (hereafter ASF-20C CTL) (Weisheimer et al., 2017). The atmospheric model used for the 4-month hindcasts is the ECMWF Integrated Forecast System Version CY41R1 and is initialized at four start dates per year (1st of Feb, May, Aug and Nov) with ERA20C land and atmospheric conditions. It uses the same lower boundary conditions for SST and sea ice as ERA-20C. Here, we only use hindcasts initialized on the 1st of November. The horizontal spectral resolution of the model of T255 is similar to ECMWF's previous

167 operational system System 4 (Molteni et al., 2011) and corresponds to a grid length of approximately

168 80 km. The model has 91 vertical levels and a top at 0.01 hPa. The ensemble has been created by

169 perturbing each member through the stochastic physics schemes to represent model uncertainties in a

170 similar way as the a-forementioned System 4.

171 To investigate the impact of Eurasian snow depth we use an additional set of perturbed hindcasts, based

172 on a 21–member subset of the ASF-20C CTL experiment (hereafter, the "Experiment" or ASF-20C

173 EXP). Each member run is initialized with different land surface conditions, sampled from the

174 neighbouring 20 years. For example, the range of land surface conditions for the 21-member ensemble

175 forecast initialised on 1st of November 1950 spans the land surface conditions of the years 1940–1960:

176 member 01 is initialized with the land surface conditions of 1940, member 02 of 1941, member 03 of

177 1942 and so forth. For the beginning and ending ten years of the hindcast dataset, the land surface

178 conditions are sampled from the closest 21 neighbouring years within the dataset. Here, land surface

179 conditions include the entire land state, including soil moisture, snow depth and soil temperatures. We

180 argue that for investigating northern hemisphere climate anomalies of the 1st of November initialization,

181 snow depth has by far the largest impact on atmospheric dynamics compared to soil moisture and soil

182 temperatures, thus allowing us to attribute the differences to snow changes. The main bulk of the

183 experiment data has a monthly resolution, and daily data is only available for selected variables and

184 three tropospheric levels. After initialization, oceanic components like SSTs and sea ice are

185 prescribed and based on observations among all members in ASF-20C CTL and ASF-20C EXP.

186 Taking advantage of the shuffled initial land conditions of ensemble members in ASF-20C EXP, we

187 subsample members with positive or negative initial Eurasian snow dipole (Figure 2). This conditional

188 sampling approach has been used when testing the sensitivity of extended range forecasts to soil

189 moisture (Koster et al., 2011; van den Hurk et al., 2012) or to snow initial conditions (Li et al., 2019;

190 Garfinkel et al., 2020). For each start date, we can identify those members with positive or negative

191 initial snow dipole indices, corresponding to different years of the shuffled land initialisation. We

192 further proceed with compositing these two selected sets. Due to the decadal variability in the November

193 snow cover, the amount of "high snow dipole members" (positive dipole index) and "low snow dipole

194 members" (negative dipole index) varies throughout the 110 years. There might be periods when a

195 majority of the neighbouring 20 years shows a positive snow dipole index and other periods when a

196 minority does. To avoid this variation of the composited ensemble size across the years, we only use

197 the five ensemble members with the most positive and most negative initial Eurasian snow dipole,

198 creating two ensemble means (each of size N=5), namely a high snow dipole ensemble-mean and low

199 snow dipole ensemble mean, for each winter through the 110-year period.

200 It should be noted that the absolute magnitude of the ensemble-mean snow differences is still changing

201 from year to year. For example, the most positive snow dipole for the period 1910–1930 might be lower

than in the time window 1980–2000, and the same applies for negative dipole indices. Due to the definition of the ASF-20C EXP, this setup is unavoidable, but it also allows for realistic magnitudes of snow forcings and for incorporating a realistic natural variability into the experiment. The (5-member) ensemble-mean difference (Figure 3a) displays a snow depth increase of 1-2 cm over Central and Eastern Siberia, together with a 0.2-1 cm snow depth decrease over Western Russia, as expected from the snow dipole definition. Concomitant negative anomalies (1-2 cm snow depth) nevertheless extend outside of the dipole definition domains to more northern latitudes, e.g., over Western Russia and the Russian Far East, or over the coastal mountain ranges of the North American Pacific Northwest. Note that the two domains forming the dipole are in snow transition zones, where the snow cover is rare on November 1st and shows some variability (Figure 3b-c). The dipole positive phase corresponds to anomalously high snow depths over Eastern Eurasia, where the ERA20C snow depth climatology indicates a few centimeters of snow. It also corresponds to anomalously low snow over the west of Russia, in regions with no to rare snow cover in the ERA20C November 1st climatology. The eastern domain partly covers the Mongolian Plateau region which was shown to exert a strong impact of the wintertime wave fluxes in the stratosphere (White et al., 2017).

If not stated otherwise we compute differences between the 5-member ensemble means of the "high snow dipole" and "low snow dipole" in ASF-20C-EXP as well as differences of each ensemble mean relative to the ensemble mean of ASF-20C CTL. We compute significance using a two-sided Student´s t-test.

3. Results
a. DJF NAO comparison

Figure 1b shows the time series of the normalized reconstructed (i.e., based on station data), reanalysed and predicted winter NAO state for the period 1901–2010. Unsurprisingly, the ensemble means of the ASF-20C CTL and ASF-20C EXP hindcasts show reduced temporal variance compared to the observation-based NAO datasets. However, single realizations and member spread of the CTL and EXP runs cover the whole range of variability displayed by the observation-based product (see also Supplementary Figure S2).

The correlation between the ERA-20C and CRU NAO index is 0.83, indicating that the EOF approach is a good approximation of the station-based index. It should be noted that the DJF average has a higher correlation between hindcasts and reanalyses than the individual months within the season (see Supplementary Table S1).

The ASF-20C CTL ensemble mean DJF hindcasts achieves an overall correlation of 0.33 with the CRU NAO reconstruction for the complete time period, with ASF-20C EXP having a nearly identical correlation (0.34). This near-identical correlation is expected given that the land state perturbations

across the 21 members are two-sided. Differences between the predicted NAO index of ASF-20C CTL and EXP ensemble means are generally small, with the NAO indices having the same sign during most winters. The correlation between CTL and EXP is 0.8 for the 110-year period. The slightly stronger variability of ASF-20C EXP can partly be attributed to the reduced ensemble size.

Contrasting the (initial) high-dipole and low-dipole composites constructed from the ASF-20C EXP ensemble, we see decadal variability in the difference of winter-mean NAO (Figure 1c&d). The first two decades of the 20th-century are characterized by rather strong negative NAO responses to a strong positive snow dipole. This is followed by two decades spanning the early twentieth century Arctic warming (Polyakov et al., 2003), which shows the opposite response: A strongly positive west-east snow depth gradient, as depicted in Figure 3, leads to more positive NAO-like states compared to a weak west-east snow depth gradient. After several decades with changing responses to the snow anomaly between the two ensembles, eventually the 21st-century starts with a weak negative NAO response to a strong positive snow dipole. Averaged over the whole period, the high snow dipole ensemble shows a slightly stronger negative NAO response: 51 cases of positive NAO response versus 59 cases of negative NAO response. For more extreme NAO states (1 SD exceedance), the difference is more pronounced: 18 versus 29, and for 2 SD exceedance, 2 versus 9. Possible reasons for the decadal response to the snow forcing will be considered in the discussion section.

b. Regression analysis

Previous studies showed that regressing observed boreal winter zonal-mean temperature and zonal wind anomalies onto an observed Eurasian autumn snow index reveals a significant stratospheric warming and slow-down of the polar vortex starting in November, migrating down towards the tropopause until February (Wegmann et al., 2020). A similar relation between Eurasian snow and the polar stratosphere can be found in the dataset used here.

Figure 4 shows a strongly reduced polar vortex for the ERA20C autumn to winter climate anomalies regressed on the November snow dipole index. The zonal wind anomalies in the troposphere highlight a weakened polar jet and an increased subtropical jet, especially in January and February. The concurrent polar stratospheric warming signal moves towards the upper troposphere throughout the winter months, with peak warming at around 100 hPa in February.

Spatially, pressure anomalies regressed onto the November snow dipole index reveal that the geographical center of the stratospheric warming is located over the Canadian Arctic (Figure 5). Tropospheric pressure differences highlight a strong ridging over Western Russia and the Ural Mountains in December, which subsequently over the course of winter is shifted more towards Greenland and the Northern North Atlantic region, reflecting a negative NAO-like atmospheric state. This state is further supported by negative DJF SLP anomalies over Southern Europe and the Mediterranean region. Downstream of the Eurasian snow signal, a negative SLP anomaly is found over

273   the Northern North Pacific. The question remains, if these patterns derived by the regression analysis

274   are a result of co-variability, common climate drivers or causal physical processes.

275   c. **Spatial anomalies in the experiment**

276   In the following, we investigate the spatial differences in the atmospheric response associated with the

277   high and low snow dipole ensemble means of ASF-20C EXP, focusing on the initial response in

278   December as well as the average DJF response, as the November response is not yet significant for

279   almost all climate variables.

280   Figure 6a&b shows stratospheric geopotential heights anomalies at 10 hPa. In December, a significant

281   negative anomaly formed above Eurasia, corresponding to a polar vortex displacement toward the

282   Eurasian sector and a high over Alaska (albeit not significant), as commonly found during stratospheric

283   warming events. Over the course of the winter, this pattern develops into increased geopotential heights

284   over the Arctic with significantly reduced geopotential heights over the extratropics, albeit only

285   significant over Southern Europe and the Caucasus.

286   To better understand the wave activity flux into the stratosphere, we investigated the meridional eddy

287   heat flux at 100 hPa, which is proportional to the vertical component of the wave activity flux (Figure

288   6c): it highlights a wave train of circumpolar anomalies in December (hence, following the surface

289   signal forcing in November) with significant positive anomalies over the Ural mountains, eastern North

290   Pacific and the European part of the North Atlantic and negative anomalies over Central and Northern

291   Europe and along the North American Pacific coast. The average DJF response highlights a circumpolar

292   wave-train but shows significant anomalies only for the increased northward heat flux over the northern

293   North Atlantic.

294   Tropospheric circulation anomalies are depicted for geopotential heights at 500hPa in Figure 6e&f. In

295   December, a strong positive anomaly is located over the Barents-Kara Sea sector, with significantly

296   negative anomalies up- and downstream. A second region of positive anomalies emerges at the

297   Canadian Atlantic coast. Both regions match the significant positive anomalies in the 100 hPa heat flux

298   well. The averaged DJF anomalies highlight a negative mid-tropospheric NAO signal with significantly

299   increased geopotential heights above Greenland and Iceland.

300   Sea level pressure anomalies largely mirror the 500 hPa geopotential height anomalies. The averaged

301   DJF pattern only shows significant positive anomalies over the northern North Atlantic, but still projects

302   onto a meridional pressure gradient characteristic of a negative NAO anomaly (Fig. 6h). It is important

303   to note, that the absolute difference is rather small compared to interannual SLP variability. Anomalies

304   between the two ensemble-means are less than 1 hPa. Even though this number can be assumed to be

305 smaller than in observational datasets due to the ensemble averaging process, it only constitutes about
306 15% of the average 1901–2010 DJF SLP standard deviation over the Euro-Atlantic sector.

307 Due to its large variability, composites of the near-surface temperature are largely non-significant
308 (Figure 6i&j). Yet, in December a clear cooling signal emerges over Central and Eastern Eurasia, as
309 expected from the location of the positive snow anomalies at the time of forecast initialization. At the
310 same time, eastern North America and south-eastern Europe show significant positive temperature
311 anomalies, a result of northward heat advection at the eastern flanks of low-pressure anomalies (Figure
312 6g). Averaged DJF 2m temperatures are significant only for Greenland and Eastern Eurasia, with the
313 cooling over the latter a direct result of the persistence of the anomalously high initial snowpack.

314
315   **d. Vertical anomalies in the experiment**
316 To get a better understanding on how the different land initial conditions impact the vertical distribution
317 of temperature and zonal wind, Figure 7 shows meridional cross-section of the zonal-mean anomalies
318 of zonal wind and temperatures from November to February.

319 While November anomalies (Figure 7) are overall insignificant, a strong snow dipole is associated with
320 an increased polar vortex and cooler stratosphere. In December, zonal wind anomalies are indicative of
321 the tropospheric subtropical jet shifted northward concurrent with a weak Arctic surface warming.
322 Changes are substantial in January, when the stratospheric polar vortex is significantly weakened, with
323 a slight increase in westerlies in the mid-troposphere. The corresponding temperature anomalies show
324 a widespread stratospheric warming and negative anomalies in the lower Arctic troposphere. Eventually
325 in February, the slow-down of westerlies is predicted to reach all the way down from the stratosphere
326 into the troposphere. On the southern flank of these negative zonal wind anomalies, westerly winds are
327 increasing, especially so in the stratosphere. The stratospheric warming signal migrates downwards to
328 the lower stratosphere and tropopause layer. As the warming has migrated down, a stratospheric cooling
329 is occurring aloft.

330 As a further confirmation, polar cap heights (Supplementary Figure S3) reveal a development of
331 positive anomalies from the surface in December up to the stratosphere in January, migrating back to
332 the troposphere in February. Note that the development of these anomalies is delayed compared to the
333 one shown in the ERA20-C reanalyses (compare Figures 4 and 7) since initial atmospheric conditions
334 are identical in the perturbed ensemble members.

335
336   **e. Daily evolution of anomalies in the experiment**
337 To investigate the temporal evolution of important tropospheric anomalies, Figure 8 shows daily mean
338 500 hPa GPH anomalies (high minus low snow dipole ensembles) averaged over 60-70°N. The
339 Hovmøller diagram illustrates the Ural ridge developing only at the end of November going into

340   December and is preceding the development of the North Atlantic ridge, which is the main component

341   of the negative NAO-like feature in our results. It should also be noted that the absence of meaningful

342   anomalies during the first ten days of the composite difference again reflects the identical tropospheric

343   anomalies arising from the pre-conditions. The anomalies generated by the end of November do indeed

344   arise from the impact of snow cover differences and snow-atmosphere feedbacks.

345

346   **f.**   **Non-linearities in the snow forcing impact**

347   Two distinct non-linearities need to be considered. First, a non-linearity in the physical snow feedback:

348   adding a few centimetres of snow in a snow–covered region will not change the radiative and

349   thermodynamic properties of the already snow-covered land surface substantially (due to a saturation

350   effect) but, by contrast, removing a few centimetres of snow might remove the snow layer altogether,

351   changing drastically the albedo and thermodynamics of the surface–atmosphere boundary. This non-

352   linearity may be important for the Rossby wave generation as air flows over the uplifted isentropes

353   above the snow-covered area. The non-linear effect of snow cover saturation and the impact of the

354   relative magnitude of regional surface cooling in our experiments is addressed by Figure 9. In years

355   when the high minus low snow depth dipole EXP ensemble anomalies preceded a negative NAO

356   anomaly (see Figure 1d for indication of years), the December cooling anomaly over Eastern Eurasia is

357   much stronger than for the opposite case when it preceded a positive NAO anomaly. Concurrently, the

358   formation of a Ural ridge anomaly is much more pronounced, flanked by troughs up and downstream,

359   with positive eddy heat fluxes into the stratosphere over the Barents-Kara Sea and polar stratospheric

360   warming. This supports the notion that adding an absolute amount of snow (in either of the two

361   longitudinal domains) is not sufficient for the causal chain to be triggered. Instead, it is a large (in

362   magnitude and extent) relative surface temperature impact of the additional snow that triggers the initial

363   anomalous Rossby wave generation part of the hypothesized causal chain.

364   A second non-linearity is the asymmetrical role of the eastern and western domains of the snow dipole.

365   Our subsampling of the ASF-20C EXP simulation allows to estimate the respective roles of these two

366   domains. Interestingly, the difference between the low snow dipole ensemble mean and the CTL

367   ensemble mean for DJF sea level pressure (Figure 10) reveals a much stronger response to a negative

368   snow dipole (i.e., with high snow depths over Western Russia and low snow depths over Eastern

369   Eurasia) than to the positive snow dipole (i.e., with high snow depths over Eastern Eurasia and low

370   snow depths over Western Russia). The reason behind this is a combination of study design, the non-

371   linearity of snow cover and the snow climatology of Eurasia. In Figure 10a, we compare the effect of a

372   very non-climatological snow depth gradient to the impact of a climatological snow depth gradient and

373   as such get a very strong response in SLP anomalies. This comparison equalizes or reduces the snow

374   depth gradient and as a result very zonal flow occurs over high-latitudes. In Figure 10b, we compare

375   the effect of a slightly increased (to the climatology) snow depth gradient to the impact of a

376 climatological snow depth gradient and as such, in addition to the weak impact of snow cover increase,
377 get a weak to non-existent surface signal out of this experimental design.

378 By splitting up the 110 years of ASF-20C CTL (climatology) in two batches with high or low snow
379 depth gradient initial conditions (1st November dipole index higher or lower than 0 based on Figure 1a)
380 we can shed more light on those non-linearities and boost the signal of the high snow depth dipole EXP
381 ensemble (Figures 10c-f). If we compare the high snow dipole EXP ensemble to CTL winter after a
382 weak west-east snow depth gradients (dipole index below 0), the anomalies show slightly elevated SLP
383 over the northern North Atlantic (Fig. 10d), albeit in much lower magnitude than for the opposite
384 comparison (Fig. 10e) (see Supplementary Figure S4 for snow depth anomalies). A weak snow depth
385 gradient seems to nearly always favour zonal flow (Figs. 10c,e,f) whereas increasing the gradient needs
386 to overcome a higher threshold due to the climatology representing a natural west-east gradient already,
387 even before the experiment treatment shows its impact. Nevertheless, anomalies between the high snow
388 depth dipole and low snow depth dipole EXP ensembles show the effect of an increased west-east snow
389 depth gradient, which does in fact support the formation of more negative NAO-like states.

390 In other words, the relative snow depth changes in our model world are much larger in the western
391 domain, and as such, the western domain carries most of the signal in our analysis. A simple regression
392 analysis with the CRU DJF NAO index and ERA20C November snow depth shows a similar result
393 (Supplementary Figure S5). We find that a linear regression model using only the eastern domain snow
394 depth variability for explaining DJF NAO shows less significance than a model only using the western
395 domain snow depth variability. Using the west-east gradient shows the highest significance for
396 predicting wintertime NAO, no matter if we use ERA20C derived NAO or station-based NAO.

397 That said, with the negative dipole corresponding to lower snow depths over the eastern domain
398 (Mongolian Plateau and surroundings areas), our results are consistent with lessened wave fluxes into
399 the stratosphere over this region which is the important orographic driver of climatological upward
400 wave fluxes in winter (White et al., 2017).

401   4. **Discussion**
402 We used a set of centennial ensemble seasonal hindcasts (ASF-20C) and a complementary set with
403 perturbed land initial conditions (ASF-20C-EXP) to address some of the open questions regarding the
404 relationship between Eurasian autumn snow cover and the state of the NAO in the following winter.
405 Subsampling of the latter hindcasts set according to the initial value (on 1st of November) of a west-east
406 snow dipole over Eurasia (Gastineau et al., 2017; Han and Sun, 2018) allowed us to determine the
407 response over 110 winters.

408 The regression of stratospheric wind and temperature upon the snow dipole in ERA20C over the 1901-
409 2010 period reveals a weakened stratospheric vortex in January and February, following a positive
410 initial snow dipole. Even though the linear regression analysis represents a deterministic "single

member" approach resulting in different magnitudes and shorter response times, the seasonal evolution of the ASF-20C EXP high-low snow dipole anomalies similarly indicates a weakened polar vortex. It also supports the notion of a surface cooling over the Eastern domain anchoring a Ural ridge anomaly on its western flank in December (Figure 6e). This Ural ridge triggers an increased northward heat flux in the lower stratosphere, thereby reducing the polar vortex strength and increasing polar stratospheric temperatures. In January and February, the signal moves downwards into the troposphere where it evolves into a negative NAO anomaly. In general, these results agree with the framework proposed by Cohen et al., (2007) and the experiments with the ECMWF seasonal prediction model by Orsolini et al. (2016). The physical causal chain in our experiment is also in line with recent model studies investigating the impact of Eurasian snow on stratospheric warmings and possible surface climate anomalies (Lü et al., 2020; Cohen et al., 2021). However, it should be highlighted that the absolute ensemble-mean, time-average SLP signal, diagnosed as the conditional composite difference in ASF-20C EXP, is very small, less than 1 hPa. As mentioned before, this represents only a small fraction of the interannual SLP variability in the Euro-Atlantic region. Nevertheless, for single realisations of winter forecasts, this impact can be much higher. By design, we excluded the impact of sea ice on the NAO evolution, since SSTs and sea ice stay the same through time in all EXP members. We checked for significant tropical precipitation patterns in the high minus low anomalies for November and December as potential co-variates in driving an DJF NAO signal but found no coherent significance across tropical latitudes. As such, we exclude tropical rainfall as first order driver behind the EXP NAO response.

The role of the Ural ridge in the snow cover → NAO causal chain has been discussed and analysed in several recent studies (Peings 2019; Santolaria-Otín et al., 2020). Here we find that the Ural ridge is a pre-condition of predicted negative NAO winters in ASF-20 CTL (Supplementary Figure S6), together with a cold 2m temperature anomaly in Eastern Russia and a cold stratospheric polar vortex displaced over Eurasia, downstream of the Ural ridge. However, these initial conditions are subtracted out in the ASF-20C EXP high--low snow dipole composite difference, and we find that the composite difference indicates a reinforced Ural ridge (Figure 6e). We find the mid-troposphere Ural ridge is reinforced only at the end of November going into December, which precedes the formation of a North Atlantic ridge that prevails until February (Figure 8). This result indicates that the snowpack does indeed play a feedback role (see also Orsolini et al., 2016). Thus, we propose that the relation between the Ural ridge and Eurasian snow cover consists of a mutual interaction: the circulation anomaly associated to a pre-existing Ural ridge shovels cold polar air southwards along its eastern flank, allowing for a deeper snowpack to form over Eastern Eurasia.In addition to this process (Figure 9c), our analysis reveals that the snow cover anomaly reinforces the Ural ridge, allowing for increased wave flux into the stratosphere. This location of a tropospheric ridge interferes constructively with climatological

stationary wave-1 and wave-2 patterns (Garfinkel et al., 2010) and seems to be key for a skilled forecast of the polar winter stratosphere (Portal et al., 2021).

Furthermore, the high minus low composite highlights a subpolar North Pacific surface and mid-tropospheric low-pressure anomaly that appears first in December and remains throughout all of DJF (Figures 6,f,g,i and 10). The generation of this circulation feature was pointed out by previous studies (Orsolini and Kvamstø, 2009; Garfinkel et al., 2010; Garfinkel et al., 2020), and has been attributed to an enhanced vertical propagation of Rossby waves into the stratosphere and horizontal downstream of the cooled Eurasian land mass.

Subsampling of the experimental multi-decadal historical hindcasts (ASF-20C EXP) highlighted an interdecadal variability and non-stationarity of the snow dipole impact, despite the cancelling out of common boundary forcings such as SSTs in the composite difference. The configuration of our experiment does not allow to explain this behaviour completely; however, we can address some possible reasons. A potential influence on the decadal variability of the snow cover impact might be the precursory climate system state, promoting or counteracting the tendency for the (perturbed) snow forcing towards a given NAO state.

Surprisingly, the positive snow dipole forcing tends to favour a negative NAO signal when the climate system is "tuned" for a positive winter NAO in ERA20C, for example when high ERA20C Barents-Kara sea ice extent and La Niña SST conditions prevail (Supplementary Figure S7). This supports the idea of a clear and strong snow impact when the relative cooling anomaly in Eastern Eurasia is relatively strong and the climate state is preconditioned to a rather positive NAO-like condition. This might explain the strong positive NAO anomaly during the early twentieth century Arctic warming in Figure 1d: the period 1920–1940 was characterized by a strong positive mid-tropospheric high anomaly from Northern Europe to East Siberia (Wegmann et al., 2017a). We find that the 500 hPa anomalies between high and low snow composites show only a weak to non-existing Ural ridge for the period 1921–1940, when compared to e.g. 1991–2010 (Supplementary Figure S8). On the contrary, increased snow in an already snow covered Eastern Eurasia will not provide the same response as the pre-existing anomalies favoured by other background conditions. Rather, strong non-linearities seem to occur, which is reasonable given the non-linear thermodynamic and radiative impacts of a deeper snowpack.

On that note, we find that the relative magnitude of regional cooling compared to the existing climate state in our experiments is of crucial importance. In years when the high-low snow dipole anomalies preceeded a negative NAO, the December cooling anomaly over Eastern Eurasia is much stronger than for the opposite case (Fig. 9). Moreover, we found that in our model experiment a negative snow dipole forcing leading to a positive NAO signal has a much larger relative impact compared to the positive snow dipole resulting in a negative NAO signal, which is due to the much stronger changes in surface forcing that we impose with the negative snow dipole ensemble. Moreover, due to the Eurasian snow

climatology, a similar level of snow depth variability in the western domain will have higher impacts on the tropospheric variability. In our experimental setup, a weak snow depth gradient from west to east allows for a rather zonal circulation in the following months, with no subsequent stratospheric warming signal. Distinct model experiments are needed to understand the atmospheric feedbacks of these configurations better. However, it should be kept in mind for future studies using regression or similar statistical tools to infer about the impact of Eurasian snow cover.

As such, we find that the main driver for the proposed snow-stratosphere linkage is a large relative impact of the additional snow depth in terms of surface temperatures as well as a strong west-east snow depth gradient. Generally, our results further highlight the importance behind the land memory effect discussed by Nakamura et al. (2019), who argue for a delayed impact of snow cover via soil and surface temperatures.

Nevertheless, we are limited in analysing the impact of co-variability in the climate system over the span of the 110-year period. Additional experiments are needed to investigate the role of climate state precursors and memory effects influencing the seasonal predictions.

5. Summary and Conclusion

Centennial seasonal ensemble hindcasts were used to examine the impact of a realistically increased November Eurasian west-to-east snow depth gradient on the boreal winter climate evolution. We found evidence for the manifestation of a negative NAO signal after a strong, positive November west-to-east snow cover dipole via surface cooling, increased Ural blocking and subsequent stratospheric warming (although evolution toward a positive NAO state was also observed but less frequently, especially for NAO extremes). Including 110-years of natural Earth System variability increases the confidence in the proposed physical mechanisms behind cryospheric drivers of atmospheric variability and decreases the probability of random co-variability between snow cover and DJF NAO. Our results hence support previous hypotheses and statistical studies. The absolute surface impact was found to be small in our experimental setup, with interdecadal variability and ensemble averaging reducing the magnitude of individual events. We found the impact of our snow forcing to be strongest for climate states that will allow the snow forcing to exert a strong surface cooling.

Future studies need to address the interplay between different Earth System components in coupled seasonal prediction experiments. How important the background conditions of the climate system are before the initialization of the forecasts needs to be investigated further. Furthermore, allowing higher magnitude snow forcing (e.g., perturbing initial land states over a longer range than the neighbouring 10 years as in this study) might result in stronger stratospheric and surface signals.

Data availability:

The ERA-20C reanalysis data is publicly available (https://apps.ecmwf.int/datasets/). The NAO reconstruction is publicly available at the Climate Research Unit repository (https://crudata.uea.ac.uk/cru/data/nao/). The ASF-20C dataset is publicly available at the CEDA Archive (https://catalogue.ceda.ac.uk/uuid/6e1c3df49f644a0f812818080bed5e45). The ASF-20C experiment dataset (created by Bart van den Hurk) can be made available on the ECMWF MARS system upon request.

Author contribution:

MW and YO designed the study. MW analysed the data. AW and BvH provided the data. GL provided discussion and interpretation of the results. All authors contributed by interpreting the results and writing the paper.

Acknowledgements:

The authors thank Daniel Balting for coding advice and Judah Cohen for fruitful discussions. GL and MW received funding through BMBF for the topic "Ocean and Cryosphere under climate change" in the Program "Changing Earth - Sustaining our Future" of the Helmholtz society.

Competing Interests:

The authors declare no competing interests.

References

Athanasiadis, P. J., Bellucci, A., Scaife, A. A., Hermanson, L., Materia, S., Sanna, A., Borrelli, A., MacLachlan, C., and Gualdi, S.: A multisystem view of wintertime nao seasonal predictions, Journal of Climate, 30, 1461–1475, https://doi.org/10.1175/JCLI-D-16-0153, 2017.

Baker, L. H., Shaffrey, L. C., Sutton, R. T., Weisheimer, A., and Scaife, A. A.: An intercomparison of skill and overconfidence/underconfidence of the wintertime north atlantic oscillation in multimodel seasonal forecasts, Geophysical Research Letters, 45, 7808–7817, https://doi.org/https://doi.org/10.1029/2018GL078838, 2018.

Blunden, J., and Boyer, T.; State of the Climate in 2020, Bulletin of the American Meteorological Society, 102, S1-S475, 2021.

Cohen, J., Barlow, M., Kushner, P. J., and Saito, K.: Stratosphere–troposphere coupling and links with eurasian land surface variability, Journal of Climate, 20, 5335–5343, https://doi.org/10.1175/2007JCLI1725.1, 2007.

547   Cohen, J., and Entekhabi, D.: Eurasian snow cover variability and northern hemisphere climate
548   predictability, Geophysical Research Letters, 26, 345–348,
549   https://doi.org/https://doi.org/10.1029/1998GL900321, 1999.

550   Cohen, J., and Jones, J.: A new index for more accurate winter predictions, Geophysical Research
551   Letters, 38, https://doi.org/https://doi.org/10.1029/2011GL049626, 2011.

552   Cohen, J., and Rind, D.: The effect of snow cover on the climate, Journal of Climate, 4, 689–706,
553   https://doi.org/10.1175/1520-0442(1991)004<0689:TEOSCO>2.0.CO;2, 1991.

554   Cohen, J., Screen, J. A., Furtado, J. C., Barlow, M., Whittleston, D., Coumou, D., Francis, J., Dethloff,
555   K., Entekhabi, D., Overland, J., and Jones, J.: Recent Arctic amplification and extreme mid-
556   latitude weather, Nature Geoscience, 7, 627–637, https://doi.org/10.1038/ngeo2234, 2014.

557   Deser, C., Hurrell, J. W., and Phillips, A. S.: The role of the north atlantic oscillation in european climate
558   projections, Climate Dynamics, 49, 3141–3157, https://doi.org/10.1007/s00382-016-3502-z,
559   2017.

560   Cohen, J., Agel, L., Barlow, M., Garfinkel, C. I., and White, I.: Linking Arctic variability and change
561   with extreme winter weather in the United States. Science, 373, 1116-1121, 2021.

562   Dirmeyer, P. A., Kumar, S., Fennessy, M. J., Altshuler, E. L., DelSole, T., Guo, Z., Cash, B. A., and
563   Straus, D.: Model estimates of land-driven predictability in a changing climate from ccsm4,
564   Journal of Climate, 26, 8495–8512, https://doi.org/10.1175/JCLI-D-13-00029.1, 2013.

565   Diro, G. T., and Lin, H.: Subseasonal Forecast Skill of Snow Water Equivalent and Its Link with
566   Temperature in Selected SubX Models. Weather and Forecasting, 35(1), 273-284, 2020.

567   Douville, H., Peings, Y., and Saint-Martin, D.: Snow-(N)AO relationship revisited over the whole
568   twentieth century, Geophysical Research Letters, 44, 569–577,
569   https://doi.org/https://doi.org/10.1002/2016GL071584, 2017.

570   Dunstone, N., Smith, D., Scaife, A., Hermanson, L., Eade, R., Robinson, N., Andrews, M., and Knight,
571   J.: Skilful predictions of the winter North Atlantic Oscillation one year ahead, Nature
572   Geoscience, 9, 809–814, https://doi.org/10.1038/ngeo2824, 2016.

573   Dutra, E., Schär, C., Viterbo, P., and Miranda, P. M. A.: Land-atmosphere coupling associated with
574   snow cover, Geophysical Research Letters, 38,
575   https://doi.org/https://doi.org/10.1029/2011GL048435, 2011.

576   Fletcher, C. G., Hardiman, S. C., Kushner, P. J., and Cohen, J.: The dynamical response to snow cover
577   perturbations in a large ensemble of atmospheric gcm integrations, Journal of Climate, 22,
578   1208–1222, https://doi.org/10.1175/2008JCLI2505.1, 2009.

579 Furtado, J. C., Cohen, J. L., Butler, A. H., Riddle, E. E., and Kumar, A.: Eurasian snow cover variability
580   and links to winter climate in the CMIP5 models, Climate Dynamics, 45, 2591–2605,
581   https://doi.org/10.1007/s00382-015-2494-4, 2015.

582 Furtado, J. C., Cohen, J. L., and Tziperman, E.: The combined influences of autumnal snow and sea ice
583   on Northern Hemisphere winters, Geophysical Research Letters, 43, 3478–3485,
584   https://doi.org/https://doi.org/10.1002/2016GL068108, 2016.

585 Garfinkel, C. I., Hartmann, D. L., and Sassi, F.: Tropospheric precursors of anomalous northern
586   hemisphere stratospheric polar vortices, Journal of Climate, 23, 3282–3299,
587   https://doi.org/10.1175/2010JCLI3010.1, 2010.

588 Garfinkel, C. I., Schwartz, C., White, I. P., and Rao, J.: Predictability of the early winter Arctic
589   oscillation from autumn Eurasian snowcover in subseasonal forecast models, Climate
590   Dynamics, 55, 961–974, https://doi.org/10.1007/s00382-020-05305-3, 2020.

591 Gastineau, G., García-Serrano, J., and Frankignoul, C.: The influence of autumnal eurasian snow cover
592   on climate and its link with arctic sea ice cover, Journal of Climate, 30, 7599–7619,
593   https://doi.org/10.1175/JCLI-D-16-0623.1, 2017.

594 Ghatak, D., Frei, A., Gong, G., Stroeve, J., and Robinson, D.: On the emergence of an Arctic
595   amplification signal in terrestrial Arctic snow extent, Journal of Geophysical Research:
596   Atmospheres, 115, https://doi.org/https://doi.org/10.1029/2010JD014007, 2010.

597 Gong, G., Entekhabi, D., and Cohen, J.: Modeled northern hemisphere winter climate response to
598   realistic siberian snow anomalies, Journal of Climate, 16, 3917–3931,
599   https://doi.org/10.1175/1520-0442(2003)016<3917:MNHWCR>2.0.CO;2, 2003.

600 Han, S., and Sun, J.: Impacts of autumnal eurasian snow cover on predominant modes of boreal winter
601   surface air temperature over eurasia, Journal of Geophysical Research: Atmospheres, 123,
602   10,076-10,091, https://doi.org/https://doi.org/10.1029/2018JD028443, 2018.

603 Hardiman, S. C., Kushner, P. J., and Cohen, J.: Investigating the ability of general circulation models
604   to capture the effects of Eurasian snow cover on winter climate, Journal of Geophysical
605   Research: Atmospheres, 113, https://doi.org/https://doi.org/10.1029/2008JD010623, 2008.

606 Henderson, G. R., Peings, Y., Furtado, J. C., and Kushner, P. J.: Snow–atmosphere coupling in the
607   Northern Hemisphere, Nature Climate Change, 8, 954–963, https://doi.org/10.1038/s41558-
608   018-0295-6, 2018.

609 Hurrell, J. W., and Deser, C.: North atlantic climate variability: The role of the north atlantic oscillation,
610   Journal of Marine Systems, 79, 231–244, https://doi.org/10.1016/j.jmarsys.2009.11.002, 2010.

Jones, P. D., Jonsson, T., and Wheeler, D.: Extension to the North Atlantic Oscillation using early instrumental pressure observations from Gibraltar and south-west Iceland. International Journal of climatology, 17, 1433-1450, 1997

Kang, D., Lee, M.-I., Im, J., Kim, D., Kim, H.-M., Kang, H.-S., Schubert, S. D., Arribas, A., and MacLachlan, C.: Prediction of the Arctic Oscillation in boreal winter by dynamical seasonal forecasting systems, Geophysical Research Letters, 41, 3577–3585, https://doi.org/https://doi.org/10.1002/2014GL060011, 2014.

Koster, R. D., Mahanama, S. P., Yamada, T. J., Balsamo, G., Berg, A. A., Boisserie, M., Dirmeyer, P. A., Doblas-Reyes, F. J., Drewitt, G., Gordon, C. T., Guo, Z., Jeong, J.-H., Lee, W.-S., Li, Z., Luo, L., Malyshev, S., Merryfield, W. J., Seneviratne, S. I., Stanelle, T., Van den Hurk, B., Vitart, F. and Wood, E. F.: The second phase of the Global Land–Atmosphere Coupling Experiment: Soil moisture contributions to subseasonal forecast skill. Journal of Hydrometeorology, 12(5), 805-822, 2011.

Kretschmer, M., Coumou, D., Agel, L., Barlow, M., Tziperman, E., and Cohen, J.: More-persistent weak stratospheric polar vortex states linked to cold extremes, Bulletin of the American Meteorological Society, 99, 49–60. https://doi.org/10.1175/BAMS-D-16-0259.1, 2018.

Li, F., Orsolini, Y. J., Keenlyside, N., Shen, M.-L., Counillon, F., and Wang, Y. G.: Impact of snow initialization in subseasonal-to-seasonal winter forecasts with the norwegian climate prediction model, Journal of Geophysical Research: Atmospheres, 124, 10033–10048, https://doi.org/https://doi.org/10.1029/2019JD030903, 2019.

Lü, Z., Li, F., Orsolini, Y., Gao, Y., He, S.: Understanding of European Cold Extremes, Sudden Stratospheric Warming, and Siberian Snow Accumulation in the Winter of 2017/18, Journal of Climate, Vol. 33. s.527-545, 2020.

Meehl, G. A., Richter, J. H., Teng, H,, Capotondi, A., Cobb, K., Doblas-Reyes, F., Donat, M. G., England, M. H., Fyfe, J. C., Han, W., Kim, H., Kirtman, B. P., Kushnir Y., Lovenduski, N. S., Mann, M. E., Merryfield, W. J., Nieves, V., Pegion, K., Rosenbloom, N., Sanchez, S. C., Scaife, A. A., Smith, D., Subramanian, A. C., Sun, L., Thompson, D., Ummenhofer, C. C. and Xie, S-P.: Initialized Earth System prediction from subseasonal to decadal timescales. Nat Rev Earth Environ 2, 340–357. https://doi.org/10.1038/s43017-021-00155-x, 2021.

Molteni, F., Stockdale, T., Alonso-Balmaseda, M., Balsamo, G., Buizza, R., Ferranti, L., Magnusson, L., Mogensen, K., Palmer, T. N., and Vitart, F.: The new ECMWF seasonal forecast system (System 4). ECMWF Technical Memorandum #656, 2011.

643 Moore, G. W. K., and Renfrew, I. A.: Cold European winters: Interplay between the NAO and the East
644   Atlantic mode, Atmospheric Science Letters, 13, 1–8.
645   https://doi.org/https://doi.org/10.1002/asl.356, 2012.

646 Nakamura, T., Yamazaki, K., Sato, T., and Ukita, J.: Memory effects of Eurasian land processes cause
647   enhanced cooling in response to sea ice loss, Nature Communications, 10, 5111.
648   https://doi.org/10.1038/s41467-019-13124-2, 2019.

649 O'Reilly, C. H., Heatley, J., MacLeod, D., Weisheimer, A., Palmer, T. N., Schaller, N., and Woollings,
650   T.: Variability in seasonal forecast skill of Northern Hemisphere winters over the twentieth
651   century, Geophysical Research Letters, 44, 5729–5738,
652   https://doi.org/https://doi.org/10.1002/2017GL073736, 2017.

653 O'Reilly, C. H., Weisheimer, A., MacLeod, D., Befort, D. J., and Palmer, T.: Assessing the robustness
654   of multidecadal variability in Northern Hemisphere wintertime seasonal forecast skill,
655   Quarterly Journal of the Royal Meteorological Society, 146, 4055–4066,
656   https://doi.org/https://doi.org/10.1002/qj.3890, 2020.

657 Orsolini, Y. J., Senan, R., Balsamo, G., Doblas-Reyes, F. J., Vitart, F., Weisheimer, A., Carrasco, A.,
658   and Benestad, R. E.: Impact of snow initialization on sub-seasonal forecasts, Climate
659   Dynamics, 41, 1969–1982, https://doi.org/10.1007/s00382-013-1782-0, 2013.

660 Orsolini, Y. J., Senan, R., Vitart, F., Balsamo, G., Weisheimer, A., and Doblas-Reyes, F. J.: Influence
661   of the Eurasian snow on the negative North Atlantic Oscillation in subseasonal forecasts of the
662   cold winter 2009/2010, Climate Dynamics, 47, 1325–1334, https://doi.org/10.1007/s00382-
663   015-2903-8, 2016.

664 Parker, T., Woollings, T., Weisheimer, A., O'Reilly, C., Baker, L., and Shaffrey, L.: Seasonal
665   predictability of the winter north atlantic oscillation from a jet stream perspective, Geophysical
666   Research Letters, 46, 10159–10167, https://doi.org/https://doi.org/10.1029/2019GL084402,
667   2019.

668 Peings, Y.: Ural blocking as a driver of early-winter stratospheric warmings, Geophysical Research
669   Letters, 46, 5460–5468, https://doi.org/https://doi.org/10.1029/2019GL082097, 2019.

670 Peings, Y., Brun, E., Mauvais, V., and Douville, H.: How stationary is the relationship between Siberian
671   snow and Arctic Oscillation over the 20th century?, Geophysical Research Letters, 40, 183–
672   188, https://doi.org/https://doi.org/10.1029/2012GL054083, 2013.

673 Peings, Y., Douville, H., Colin, J., Martin, D. S., and Magnusdottir, G.: Snow–(N)ao teleconnection
674   and its modulation by the quasi-biennial oscillation, Journal of Climate, 30, 10211–10235,
675   https://doi.org/10.1175/JCLI-D-17-0041.1, 2017.

676 Peings, Y., Saint-Martin, D., and Douville, H.: A numerical sensitivity study of the influence of siberian
677 snow on the northern annular mode, Journal of Climate, 25, 592–607,
678 https://doi.org/10.1175/JCLI-D-11-00038.1, 2012.

679 Polyakov, I. V., Bekryaev, R. V., Alekseev, G. V., Bhatt, U. S., Colony, R. L., Johnson, M. A.,
680 Maskshtas, A. P. and Walsh, D.: Variability and trends of air temperature and pressure in the
681 maritime Arctic, 1875–2000. Journal of Climate, 16(12), 2067-2077, 2003

682 Portal, A., Ruggieri, P., Palmeiro, F. M., García-Serrano, J., Domeisen, D. I., & Gualdi, S.: Seasonal
683 prediction of the boreal winter stratosphere, Climate Dynamics, 1-22, 2021.

684 Santolaria-Otín, M., García-Serrano, J., Ménégoz, M., and Bech, J.: On the observed connection
685 between Arctic sea ice and Eurasian snow in relation to the winter North Atlantic Oscillation,
686 Environmental Research Letters, 15, 124010, https://doi.org/10.1088/1748-9326/abad57, 2021.

687 Santolaria-Otín, M., and Zolina, O.: Evaluation of snow cover and snow water equivalent in the
688 continental Arctic in CMIP5 models, Climate Dynamics, 55, 2993–3016,
689 https://doi.org/10.1007/s00382-020-05434-9, 2020.

690 Scaife, A. A., Arribas, A., Blockley, E., Brookshaw, A., Clark, R. T., Dunstone, N., Eade, R., Fereday,
691 D., Folland, C. K., Gordon, M., Hermanson, L., Knight, J. R., Lea, D. J., MacLachlan, C.,
692 Maidens, A., Martin, M., Peterson, A. K., Smith, D., Vellinga, M., Wallace, E., Waters, J. and
693 Williams, A.: Skillful long-range prediction of European and North American winters,
694 Geophysical Research Letters, 41, 2514–2519,
695 https://doi.org/https://doi.org/10.1002/2014GL059637, 2014.

696 Scaife, A. A., Karpechko, A. Y., Baldwin, M. P., Brookshaw, A., Butler, A. H., Eade, R., Gordon, M.,
697 MacLachlan, C., Martin, N., Dunstone, N., and Smith, D.: Seasonal winter forecasts and the
698 stratosphere, Atmospheric Science Letters, 17, 51–56,
699 https://doi.org/https://doi.org/10.1002/asl.598, 2016.

700 Smith, D. M., Scaife, A. A., Eade, R., and Knight, J. R.: Seasonal to decadal prediction of the winter
701 North Atlantic Oscillation: Emerging capability and future prospects, Quarterly Journal of the
702 Royal Meteorological Society, 142, 611–617, https://doi.org/https://doi.org/10.1002/qj.2479,
703 2016.

704 Song, L., & Wu, R., 2019: Intraseasonal snow cover variations over western Siberia and associated
705 atmospheric processes, Journal of Geophysical Research: Atmospheres, 124, 8994–
706 9010.Thackeray, C. W., Derksen, C., Fletcher, C. G., and Hall, A.: Snow and climate:
707 Feedbacks, drivers, and indices of change, Current Climate Change Reports, 5, 322–333,
708 https://doi.org/10.1007/s40641-019-00143-w, 2019.

Thompson, D. W. J., and Wallace, J. M.: The Arctic oscillation signature in the wintertime geopotential height and temperature fields, Geophysical Research Letters, 25, 1297–1300, https://doi.org/10.1029/98GL00950 , 1998.

Tian, B., and Fan, K.: A skillful prediction model for winter nao based on atlantic sea surface temperature and eurasian snow cover, Weather and Forecasting, 30, 197–205, https://doi.org/10.1175/WAF-D-14-00100.1, 2015.

Tyrrell, N. L., Karpechko, A. Y., and Räisänen, P.: The influence of eurasian snow extent on the northern extratropical stratosphere in a qbo resolving model, Journal of Geophysical Research: Atmospheres, 123, 315–328, https://doi.org/https://doi.org/10.1002/2017JD027378, 2018.

Tyrrell, N. L., Karpechko, A. Y., Uotila, P., and Vihma, T.: Atmospheric circulation response to anomalous siberian forcing in october 2016 and its long-range predictability, Geophysical Research Letters, 46, 2800–2810, https://doi.org/https://doi.org/10.1029/2018GL081580 , 2019.

van den Hurk, B., Kim, H., Krinner, G., Seneviratne, S. I., Derksen, C., Oki, T., Douville, H., Colin, J., Ducharne, A., Cheruy, F., Viovy, N., Puma, M. J., Wada, Y., Li, W., Jia, B., Alessandri, A., Lawrence, D. M., Weedon, G. P., Ellis, R., Hagemann, S., Mao, J., Flanner, M. G., Zampieri, M., Materia, S., Law, R. M., and Sheffield, J.: Ls3mip (V1. 0) contribution to cmip6: The land surface, snow and soil moisture model intercomparison project – aims, setup and expected outcome, Geoscientific Model Development, 9, 2809–2832, https://doi.org/10.5194/gmd-9-2809-2016 , 2016.

Vavrus, S.: The role of terrestrial snow cover in the climate system, Climate Dynamics, 29, 73–88, https://doi.org/10.1007/s00382-007-0226-0, 2007.

Wang, L., Ting, M., and Kushner, P. J.: A robust empirical seasonal prediction of winter NAO and surface climate, Scientific Reports, 7, 279, https://doi.org/10.1038/s41598-017-00353-y , 2017.

Wanner, H., Brönnimann, S., Casty, C., Gyalistras, D., Luterbacher, J., Schmutz, C., Stephenson, D. B., and Xoplaki, E.: North atlantic oscillation – concepts and studies, Surveys in Geophysics, 22, 321–381, https://doi.org/10.1023/A:1014217317898, 2001.

Wegmann, M., Orsolini, Y., Vázquez, M., Gimeno, L., Nieto, R., Bulygina, O., Jaiser, R., Handorf, D., Rinke, A., Dethloff, K., Sterin, A., and Brönnimann, S.: Arctic moisture source for Eurasian snow cover variations in autumn, Environmental Research Letters, 10, 054015, https://doi.org/10.1088/1748-9326/10/5/054015, 2015.

Wegmann, M., Brönnimann, S., and Compo, G. P.: Tropospheric circulation during the early twentieth century Arctic warming. Climate dynamics, 48, 2405-2418, 2017a.

742 Wegmann, M., Orsolini, Y., Dutra, E., Bulygina, O., Sterin, A., & Brönnimann, S.: Eurasian snow
743   depth in long-term climate reanalyses. The Cryosphere, 11, 923-935, 2017b

744 Wegmann, M., Rohrer, M., Santolaria-Otín, M., and Lohmann, G.: Eurasian autumn snow link to winter
745   North Atlantic Oscillation is strongest for Arctic warming periods, Earth System Dynamics, 11,
746   509–524, https://doi.org/https://doi.org/10.5194/esd-11-509-2020, 2020.

747 Weisheimer, A., Befort, D. J., MacLeod, D., Palmer, T., O'Reilly, C., and Strømmen, K.: Seasonal
748   forecasts of the twentieth century, Bulletin of the American Meteorological Society, 101,
749   E1413–E1426, https://doi.org/10.1175/BAMS-D-19-0019.1, 2020.

750 Weisheimer, A., Decremer, D., MacLeod, D., O'Reilly, C., Stockdale, T. N., Johnson, S., and Palmer,
751   T. N.: How confident are predictability estimates of the winter North Atlantic Oscillation?,
752   Quarterly Journal of the Royal Meteorological Society, 145, 140–159,
753   https://doi.org/https://doi.org/10.1002/qj.3446, 2019.

754 Weisheimer, A., Schaller, N., O'Reilly, C., MacLeod, D. A., and Palmer, T.: Atmospheric seasonal
755   forecasts of the twentieth century: Multi-decadal variability in predictive skill of the winter
756   North Atlantic Oscillation (Nao) and their potential value for extreme event attribution,
757   Quarterly Journal of the Royal Meteorological Society, 143, 917–926,
758   https://doi.org/https://doi.org/10.1002/qj.2976, 2017.

759 White, R. H., Battisti, D. S., & Roe, G. H.: Mongolian Mountains Matter Most: Impacts of the Latitude
760   and Height of Asian Orography on Pacific Wintertime Atmospheric Circulation, Journal of
761   Climate, 30, 4065-4082, 2017.

762 Zhang, R., Sun, C., Zhang, R., Li, W., and Zuo, J.: Role of Eurasian snow cover in linking winter-spring
763   Eurasian coldness to the autumn arctic sea ice retreat, Journal of Geophysical Research:
764   Atmospheres, 124, 9205–9221, https://doi.org/https://doi.org/10.1029/2019JD030339, 2019.

765
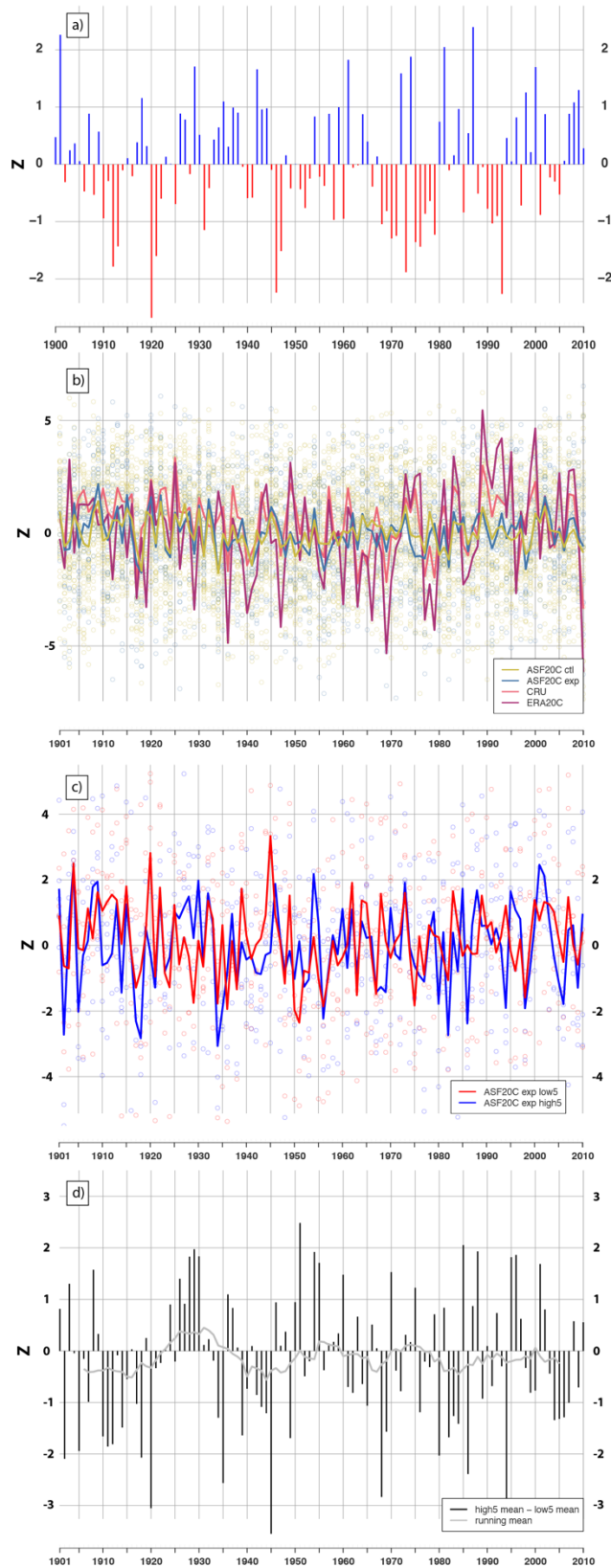
Figure 1: a) Normalized 1st of November Eurasian snow dipole index for the period 1900–2010 as derived from ERA20C. b) Normalized DJF NAO index in the CRU station-based reconstruction, ERA20C EOF-based index, ASF-20C CTL and ASF-20C EXP EOF-based index. Hollow points

769 *represent individual members, solid lines represent ensemble means or observational products. c) 5-*
770 *member DJF NAO forecasts for the high- and low-dipole members within ASF-20C EXP. Hollow points*
771 *represent individual members, solid lines represent ensemble means. d) NAO DJF state difference and*
772 *its 11-year running mean between the ASF-20C EXP high- and low-dipole ensemble mean in panel b*
773 *(51(18) cases of positive (+1 SD) NAO response, 59 (29) cases of negative (-1 SD) NAO response). For*
774 *2 SD exceedance, the number of cases is 2 vs 9.*

775

776
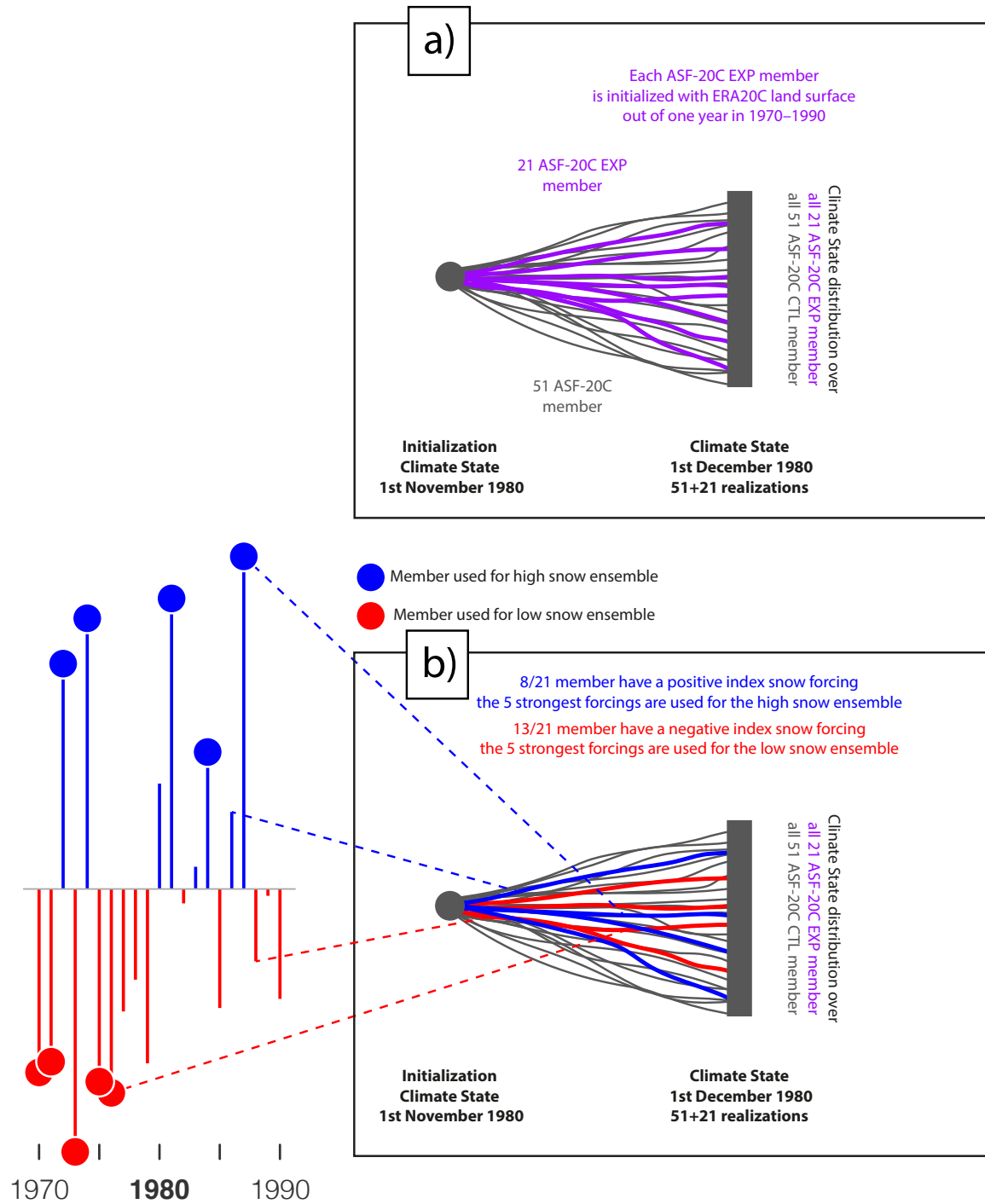
Figure 2: As an example, the schematic for a) the 1980 1st of November ASF-20C EXP initialization
and the consequent sampling of the 21 ensemble members into the high and low snow dipole ensembles.
For the 1st of November initialization, ASF-20C EXP members are initialized by land surface
conditions of the 21 surrounding 1st of November dates, in this case 1970–1990, b) Out of these 21
members, we sample individual members based on their ranking in the snow index. The five members
with the most positive snow index constitute the high snow ensemble and vice versa for the low snow
ensemble.
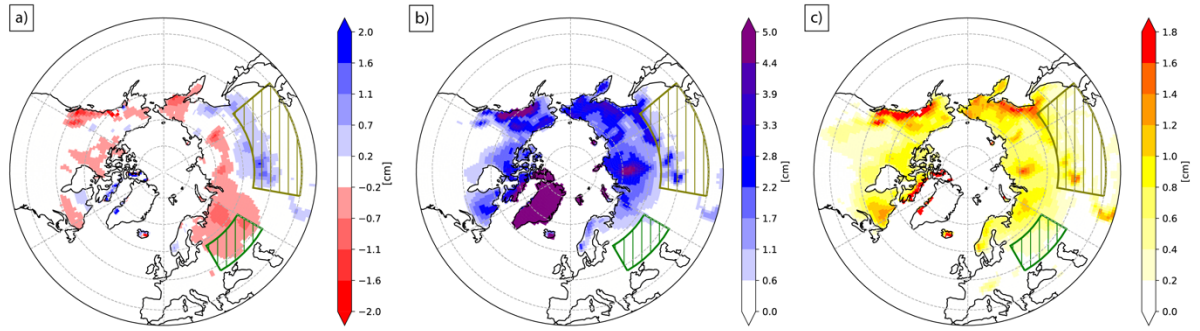
784
785 *Figure 3: a) Average (1900–2010) 1st of November snow depth difference between the high-dipole*
786 *and low-dipole ensemble. b) Average (1900–2010) 1st of November snow depth. c) Average (1900–*
787 *2010) 1st of November snow depth standard deviation. Hatched in green (olive) is the western*
788 *(eastern) domain of the snow index. All 3 plots are based on ERA20C.*
789

790

791
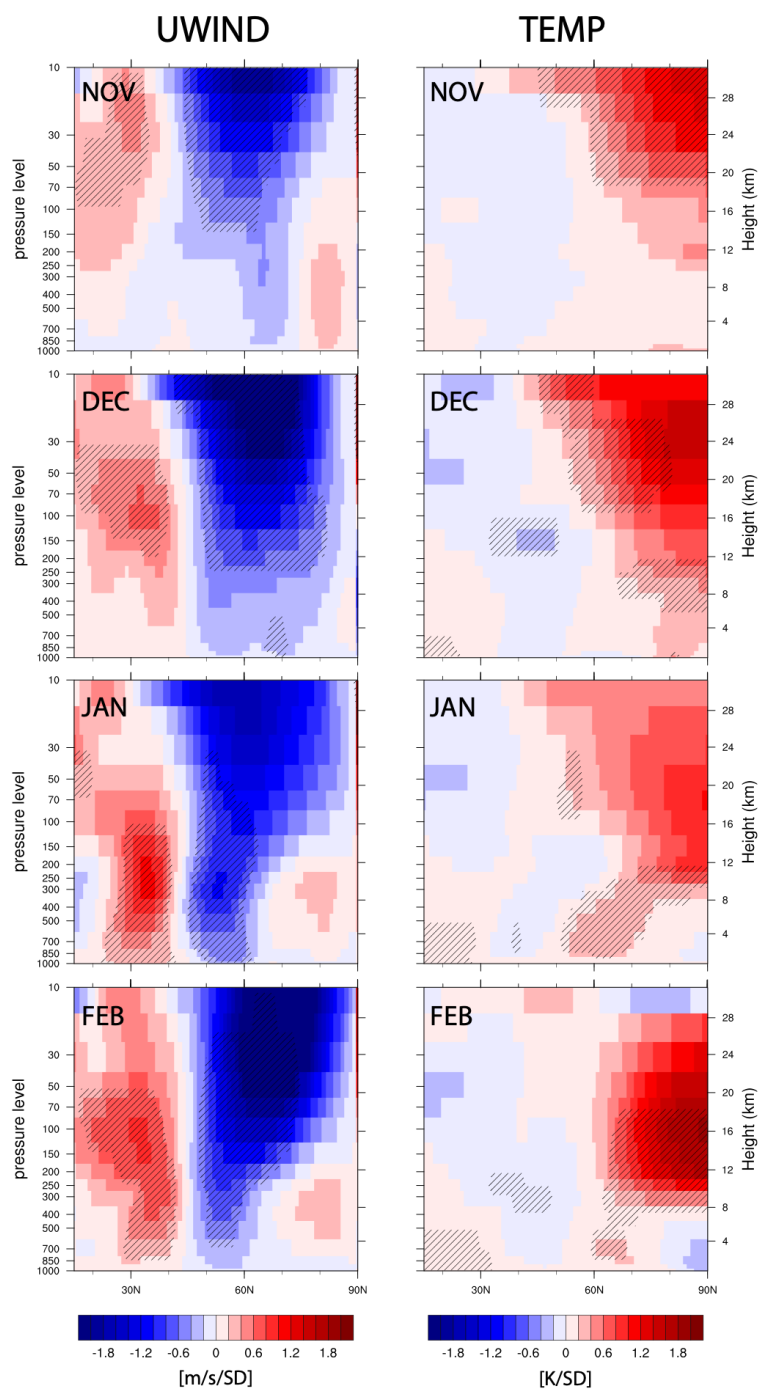
Figure 4: Zonal-mean meridional cross-section of ERA20C anomalies in temperature and zonal wind regressed onto the snow dipole index in November from ERA20C covering 1901–2010 for November, December, January and February. Shading indicates 95% significance level.

795
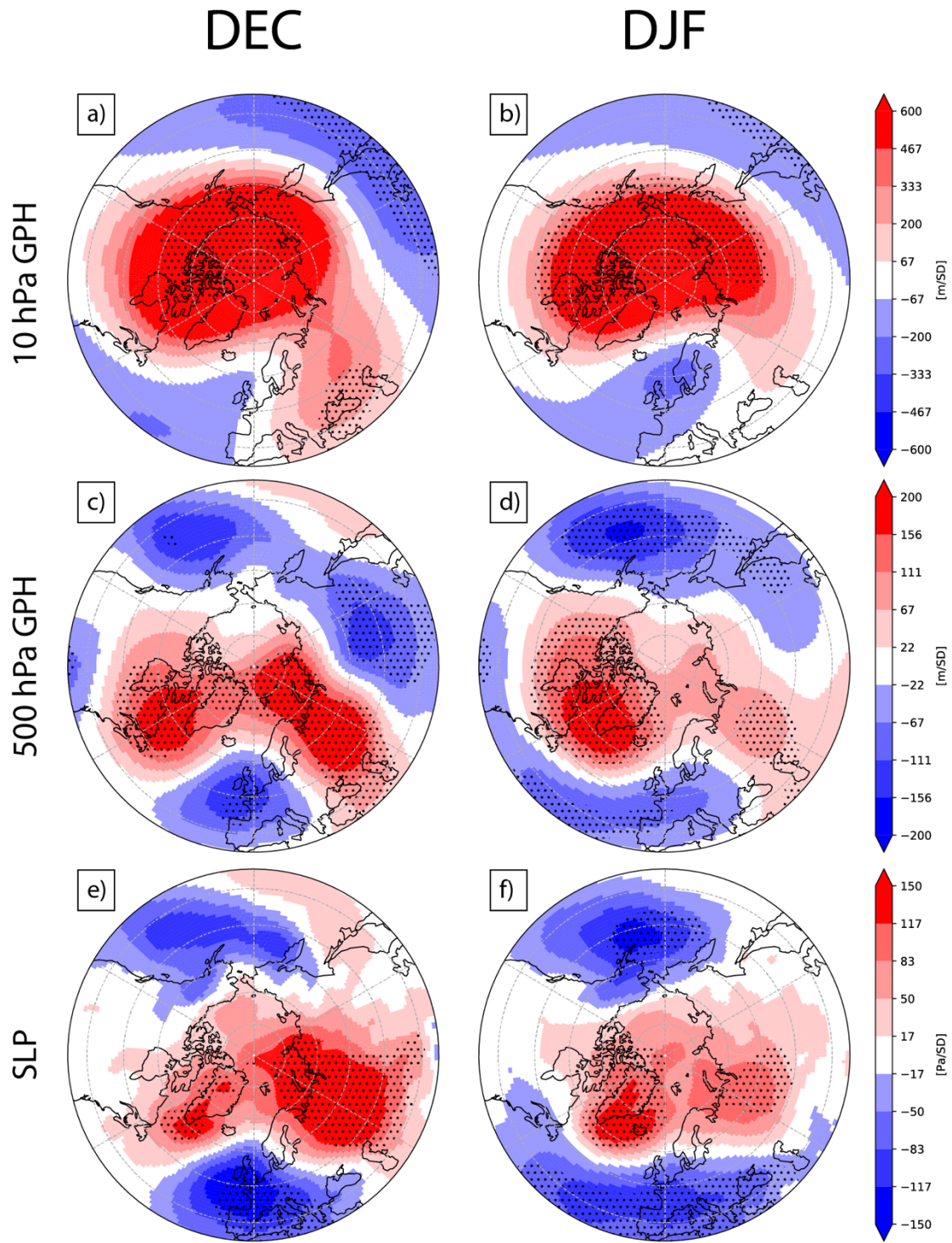
Figure 5: ERA20C anomalies of a&b)10 hPa geopotential heights, c&d) 500 hPa geopotential heights and e&f) Sea Level Pressure regressed onto the snow dipole index in November from ERA20C covering 1901–2010 for December and DJF mean. Shading indicates 95% significance level. For monthly anomalies see Supplementary Figure S9.

800
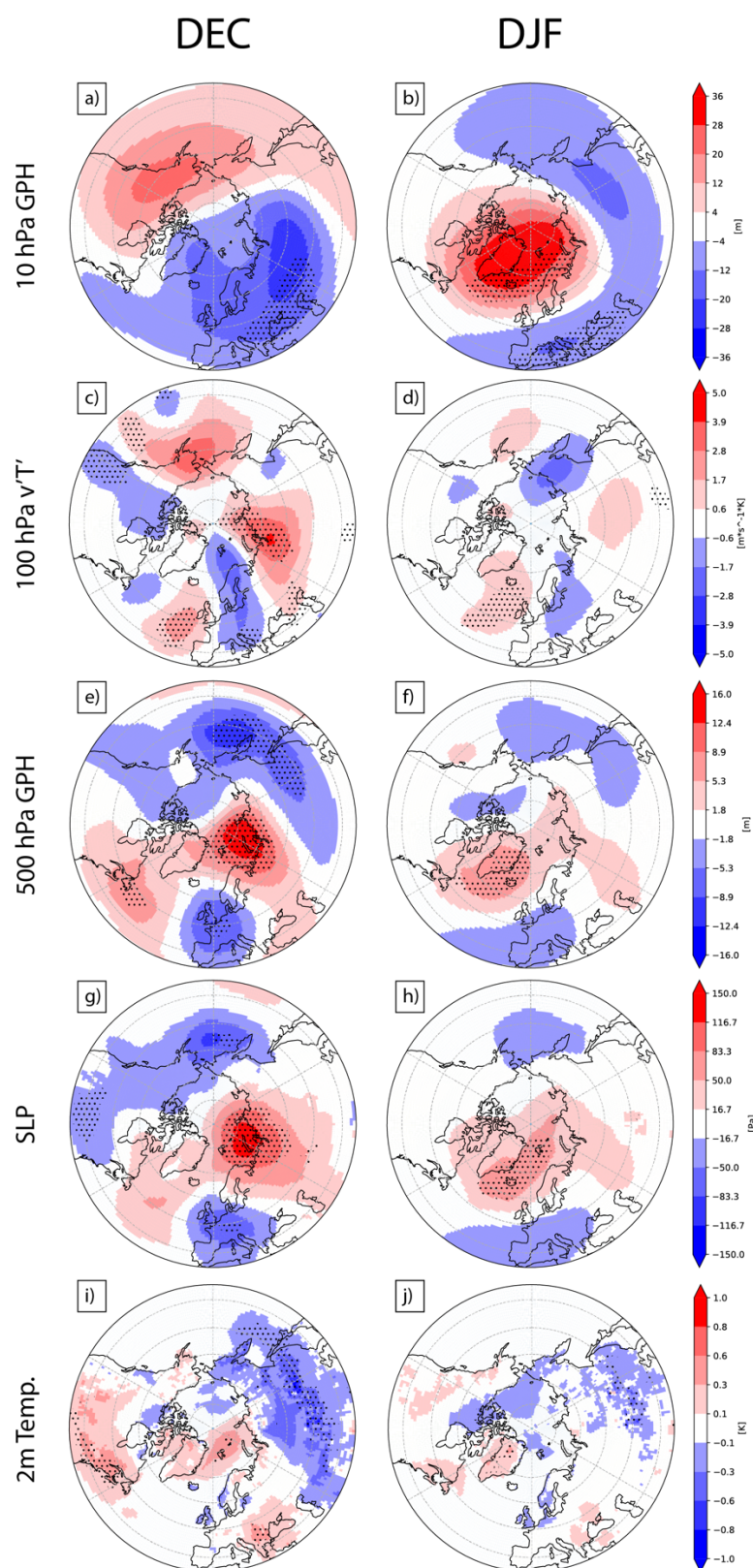
801 *Figure 6: Averaged anomalies 1901-2010 between high-dipole and low-dipole ASF-20C EXP ensemble*
802 *means for December (a,c,e,g,j), and DJF (b,d,f,i,k): a&b) 10 hPa geopotential heights, c&d) 100 hPa*
803 *meridional eddy heat flux, e&f) 500 hPa geopotential heights, g&h) sea level pressure and i&j) 2m*
804 *temperature. Stippled areas represent 90% significance. For monthly anomalies see Supplementary*
805 *Figure S10.*
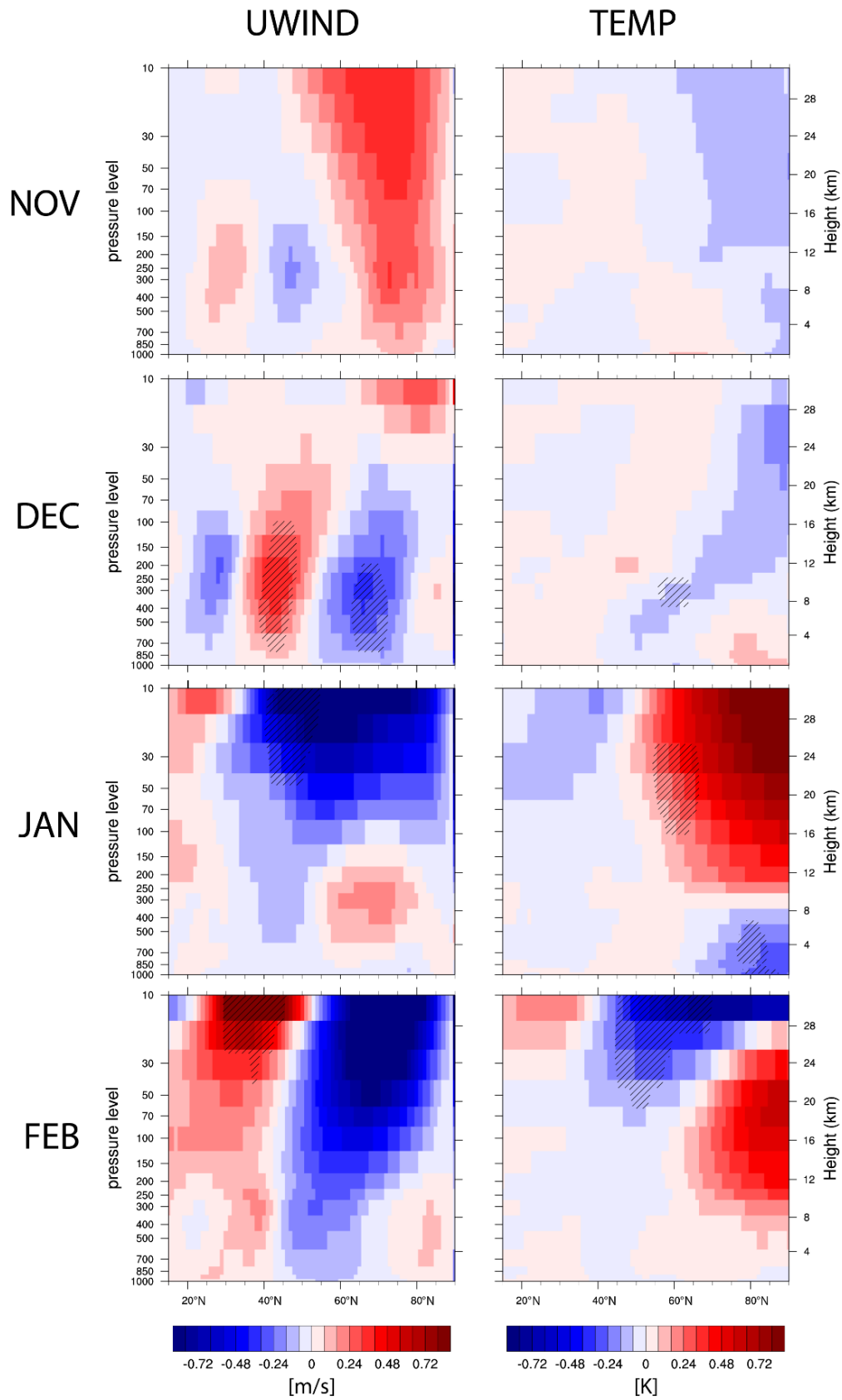
807 *Figure 7: Zonal-mean cross-section of left) zonal wind anomalies and right) temperature anomalies for*
808 *the period 1901-2010 between high-dipole and low-dipole ASF-20C EXP ensemble means. Shading*
809 *indicates 90% significance level.*

806
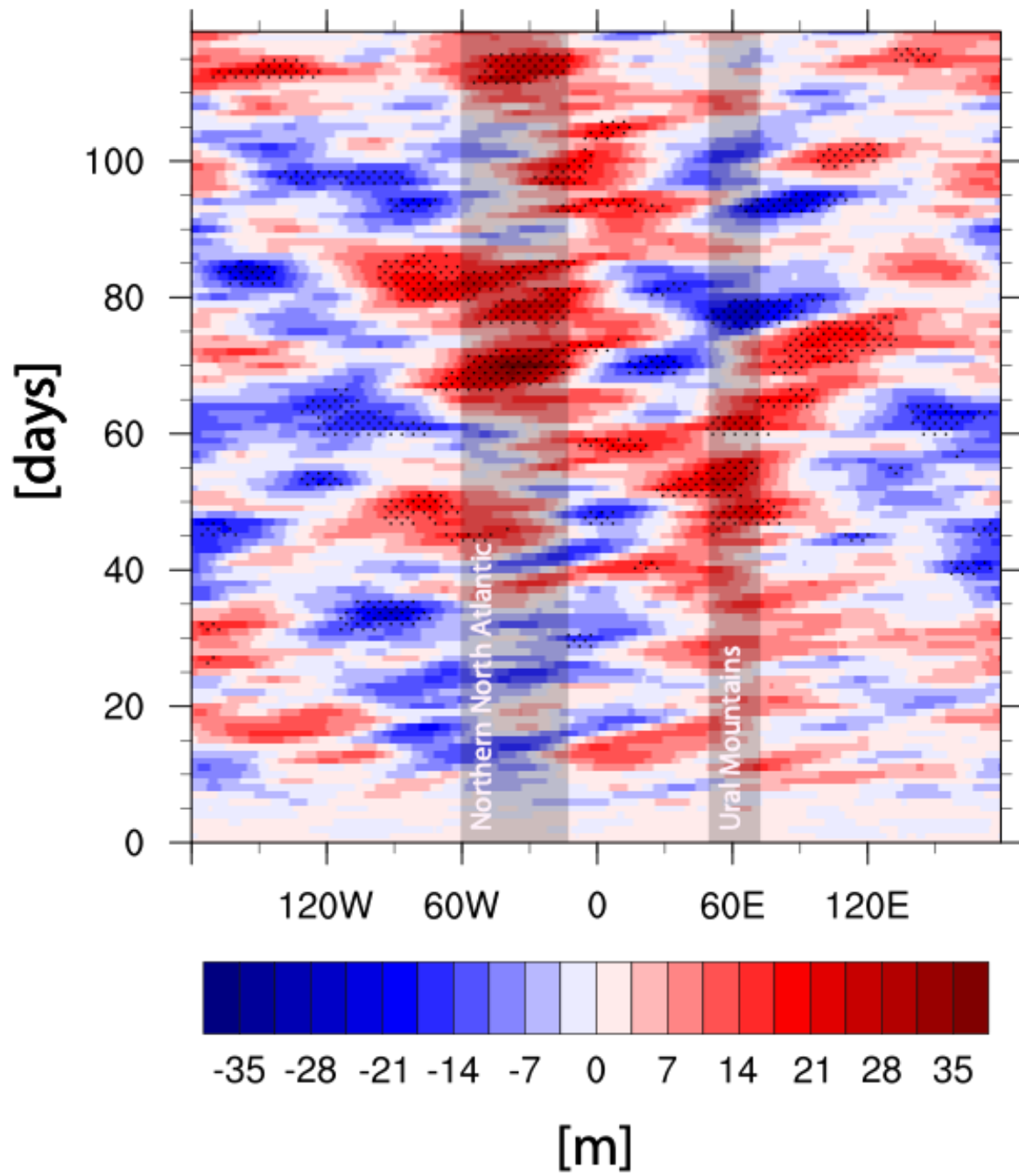
810

811 *Figure 8: Hovmøller diagram of daily mean predicted 500 hPa geopotential height anomalies for the*
812 *period 1901-2010 averaged for the latitude band 60°-70°N difference between high-dipole and low-*
813 *dipole ASF-20C EXP ensemble means. Stippled areas represent 90% significance. Days from NOV 1st*
814 *are indicated on y-axis.*

815
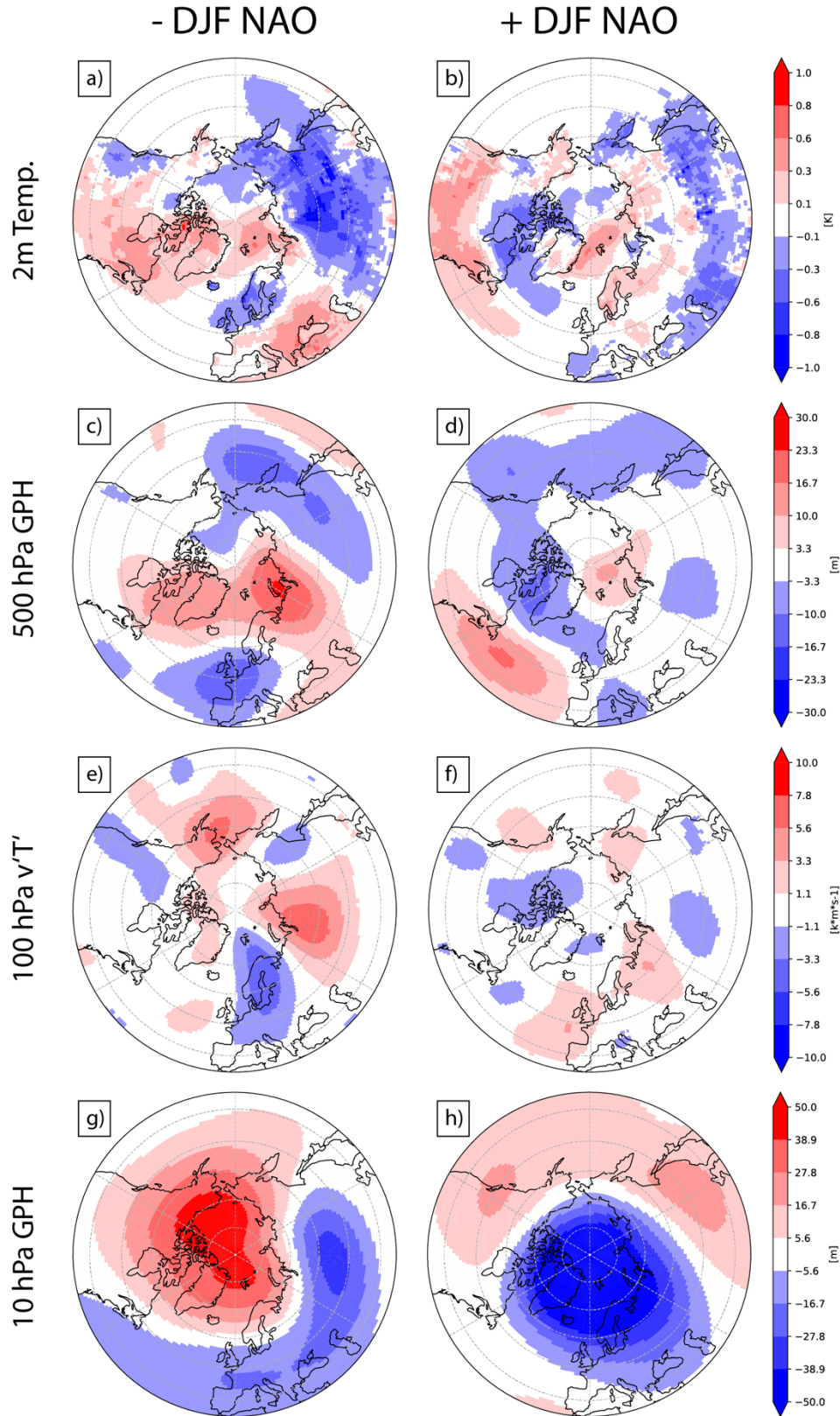
816 *Figure 9: Climate anomaly composites of predicted December fields after which a positive snow dipole*
817 *forcing preceeded a negative DJF NAO signal (a,c,e,g) or a positive DJF NAO signal (b,d,f,i)(selection*
818 *of years based on Figure 1d): a&b) 2m temperature, c&d) 500 hPa geopotential heights, e&f) 100hPa*
819 *meridional eddy temperature flux, g&h) 10 hPa geopotential heights. Anomalies are based on ASF-*
820 *20C EXP high-low snow dipole ensemble mean data.*

821
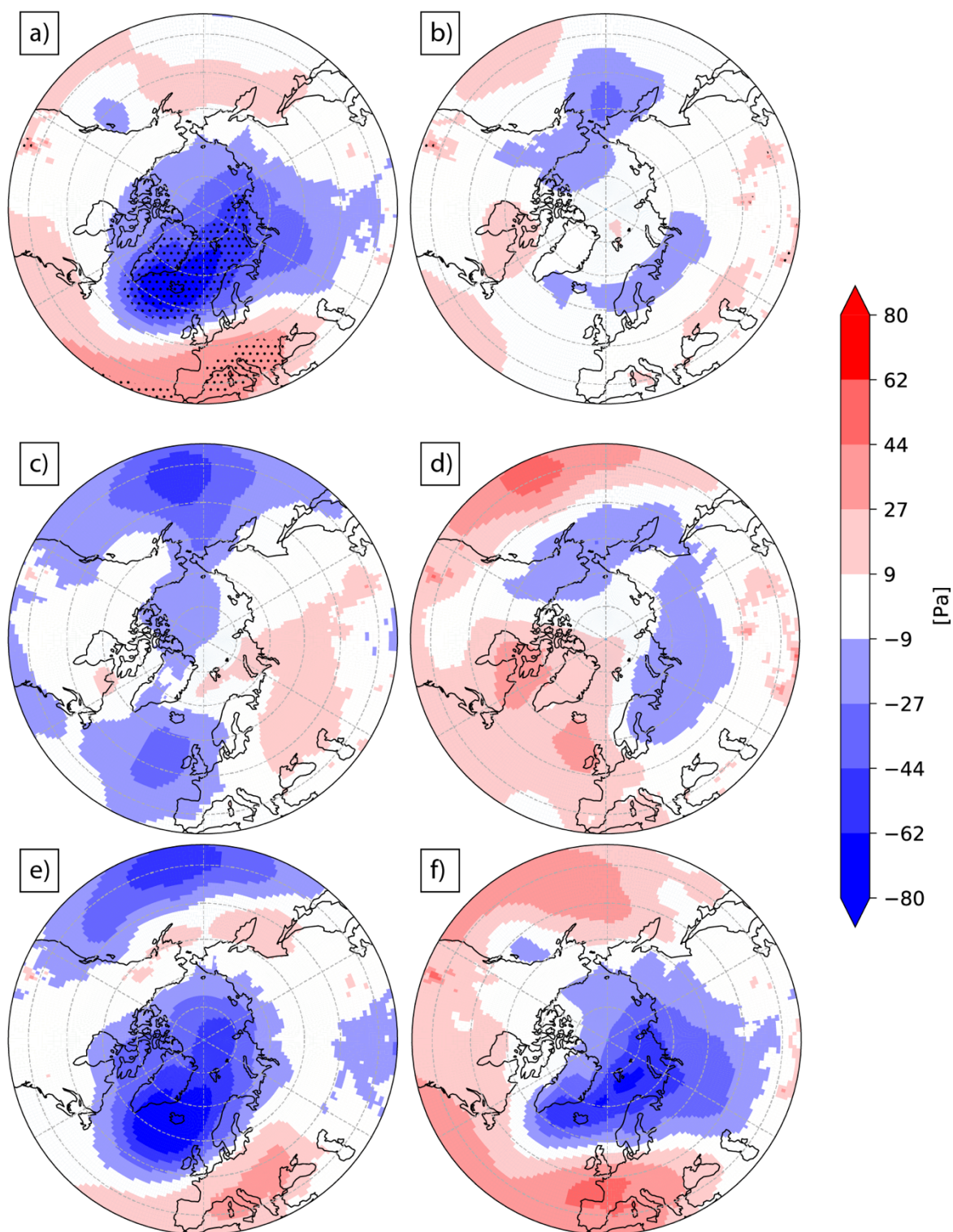
Figure 10: Mean sea level pressure [Pa] DJF anomalies for the period 1901-2010 between a) low-dipole ASF-20C EXP ensemble mean and ASF-20C CTL ensemble mean (subsampled from 21 CTL members) and b) high-dipole ASF-20C EXP ensemble mean and ASF-20C CTL ensemble mean (subsampled from 21 CTL members). Stippled areas represent 90% significance. c) Represents differences between high-dipole ASF-20C EXP ensemble mean and ASF-20C CTL ensemble mean DJF seasons after positive snow dipole in November (see Figure 1a). d) as c) but for DJF seasons after negative snow dipole November. e) as c) but for difference between the low-dipole ASF-20C EXP ensemble mean and ASF-20C CTL ensemble mean DJF seasons after negative snow dipole in

830 *November. f) as e) but for the ASF-20C CTL ensemble mean DJF seasons after positive snow dipole in*
831 *November.*